Stabilizing silver window electrodes for organic photovoltaics using a mercaptosilane monolayer

Jaemin Lee[1], Marc Walker[2], Silvia Varagnolo[1], Steven Huband[2] and Ross A. Hatton[1]*

[1]Department of Chemistry, University of Warwick, CV4 7AL, Coventry, United Kingdom

[2]Department of Physics, University of Warwick, CV4 7AL, Coventry, United Kingdom

*E-mail: Ross.Hatton@warwick.ac.uk

ABSTRACT

A single layer of the bifunctional molecule 3-mercaptopropyltrimethoxysilane is shown to be remarkably effective at improving the stability of optically thin silver film electrodes towards spontaneous morphological change and oxidation by airborne sulfur. Inclusion of this layer in the novel transparent electrode; WO_3 (30 nm) / silver (13 nm) / sol-gel ZnO (27 nm), at the silver / ZnO interface improves the efficiency of organic photovoltaic devices using this electrode by 20%, such that the power conversion efficiency is very close to that achievable using a conventional indium-tin oxide glass electrode; 9.6 % ± 0.2 % *vs* 10.0 % ± 0.3 %, with the advantage that the silver electrode has a sheet resistance one third that of the ITO glass (~4 Ohms sq^{-1}). The mercaptosilane monolayer is also shown to retard silver diffusion into the ZnO layer whilst imparting a favorable ~400 meV reduction in electrode work function. In addition to its utility inside the device, this molecular layer is shown to be useful for improving the

stability of the silver film electrodes in top-illuminated semi-transparent photovoltaics, since it can be deposited directly onto a completed device from the vapor phase.

KEY WORDS

Monolayer, organic solar cell, organic photovoltaic, transparent electrode, silver electrode, 3-mercaptopropyltrimethoxysilane, work function, silane

TOC GRAPHIC

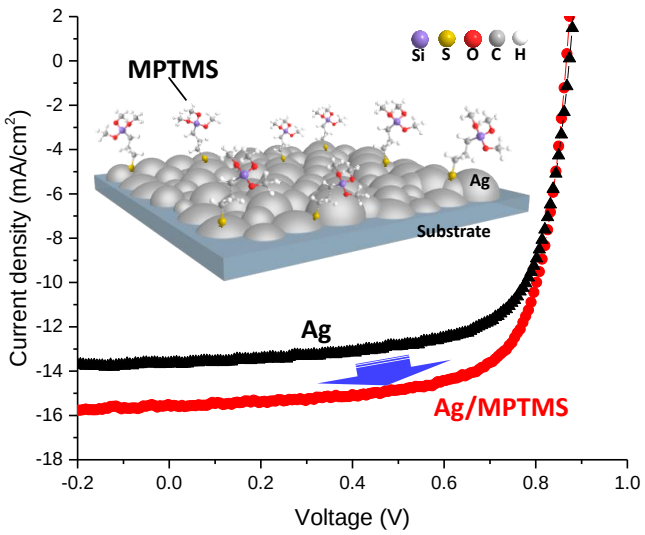

INTRODUCTION

Molecular monolayers have been widely used to powerful effect in organic photovoltaics (OPVs), light-emitting diodes and transistors, primarily to engineer the work function and surface energy of the electrodes,[1-4] but also as nucleation layers for the fabrication of transparent metal films on glass and plastic substrates.[5,6] For OPVs optically thin silver (Ag) films deposited by vacuum evaporation are particularly attractive as the basis for the transparent electrode because Ag has a very low extinction coefficient and the highest electrical conductivity amongst metals.[7-9] Vacuum evaporation is the deposition method of choice because it is proven as a low cost method for thin metal film deposition used in the food packaging industry. Whilst Ag is a relatively expensive metal, it is possible that in the context of OPVs it can be easily recovered and recycled by incinerating the entire device at the end of its useful life.[10] One compound that has proved particularly useful as a nucleation layer for Ag, and other coinage metals, is the small molecule 3-mercaptopropyltrimethoxysilane (MPTMS) because monolayers of this molecule form a strong chemical bond to the substrate via the siloxane linkage and immobilize condensing Ag atoms by forming a strong thiolate linkage.[11] For this reason MPTMS is the nucleation layer used for the fabrication of optically thin Ag films on glass in this study (Supporting Information (SI) Figure 1). Without an adhesion layer optically thin Ag films on glass, and the technologically important flexible transparent substrates polyethylene terephthalate (PET) and polyethylene naphthalate (PEN), are morphologically very unstable even at room temperature, with changes in the optical properties occurring on the time scale of minutes after metal deposition (Reference 12, SI Figures S2 and S3). Even when using a metal nucleation layer, detrimental morphological change still occurs on the time scale of weeks (SI Figures S4), which is a serious problem for their practical application in OPVs. Additionally, thin Ag films are very susceptible to oxidation in ambient

air, particularly by sulphurous compounds which degrade electrode sheet resistance, which is a problem if the electrode is stored in air prior to integration into a device.[13]

Herein we show that a single layer of MPTMS molecules deposited onto the surface of optically thin Ag film electrodes is remarkably effective at stabilizing them towards spontaneous changes in morphology and oxidation by airborne sulfur. When used as the transparent electrode in high performance OPVs the very low thickness of the MPTMS layer means it does not contribute to device series resistance or parasitic absorption of light. The utility of this ultra-thin layer is demonstrated in the context of a novel oxide-metal-oxide electrode comprising an optically thin silver film sandwiched between tungsten oxide and zinc oxides layers, where it stabilizes the silver - ZnO interface. Oxide-metal-oxide electrodes with the well-known architectures; WO_3 / Ag / WO_3 and MoO_3 / Ag / MoO_3 are limited by the conductivity of evaporated WO_3 and MoO_3 respectively, because the thickness of the oxide layer interfacing the organic photoactive layer is typically less than that needed for optimal optical performance.[6] The much higher conductivity of sol-gel processed ZnO used herein removes this constraint. Additionally, the electrode reported herein enables OPV fabrication with an inverted device architecture, which is well-known to yield more stable OPV devices. Herein we also demonstrate how we can utilize the ultra-thin MPTMS layer as a capping layer in semi-transparent OPVs to improve device stability.

MPTMS layer characterisation

In this study optically thin Ag films were deposited by thermal evaporation onto glass substrates modified with an MPTMS nucleation layer as detailed in the Experimental section and SI Figure S1. Using this method the surface roughness and sheet resistance of a 9 nm Ag

film is ~1 nm (Figure 1) and ~6.5 Ohms sq^{-1} respectively which is comparable to the lowest sheet resistance reported for a Ag film of this thickness using any nucleation layer including polyethylenimine (PEI) adhesion layer.[13,14] MPTMS derivatization of the top surface of these Ag electrodes was then performed for 2 hours in air at 100 ºC in a sealed glass crystalizing dish using the vapour phase deposition method, which avoids the use of a solvent. Figure 1a depicts the MPTMS nucleation layer and the MPTMS monolayer capping the Ag film. The subject of this study is the role of the latter. To avoid confusion the MPTMS nucleation layer is referred to as the 1st MPTMS layer and the MPTMS capping layer as the 2nd MPTMS layer, reflecting the order in which they are deposited. After the 2nd MPTMS deposition the surface roughness increases from 0.9 ± 0.1 nm (Figures 1b and SI Figure S4) to 1.5 ± 0.1 nm (Figures 1c and SI Figure S4), which indicates that either the MPTMS layer is of non-uniform thickness and/or that the metal film morphology has changed due to heating during the MPTMS deposition. Close inspection reveals that the increase in surface roughness is due to low density of isolated low-aspect ratio mounds covering < 8 % of the film surface area. It is evident from the morphology and current mapping images of the conductive atomic force microscope (C-AFM) in Figures 1(c) and (d) that these surface protrusions are > 2 nm higher than the surrounding electrode surface and are much more insulating than the other 92 % of the surface so they cannot be mounds of Ag. MPTMS has saturated bonds and so the mechanism of charge transport through this material is off-resonant tunnelling which is characterised by a sharp exponential decrease in conductance with increasing thicknesses.[15] Consequently for MPTMS layer thicknesses > 1 nm (equivalent to the thickness of one monolayer: 0.8-0.9 nm) charge transport to and from the electrode will be impeded.[15] Given the well-known propensity of trimethoxysilanes to polymerise in the presence of trace water,[16] these isolated mounds are attributed to locally polymerised MPTMS. The surface roughness over the remaining 92 % of the substrate is 1.1 nm ± 0.1 nm, which is not significantly different to that of the bare Ag (0.9

± 0.1 nm), indicating that the thickness of the MPTMS layer is uniform over the vast majority of the Ag surface.

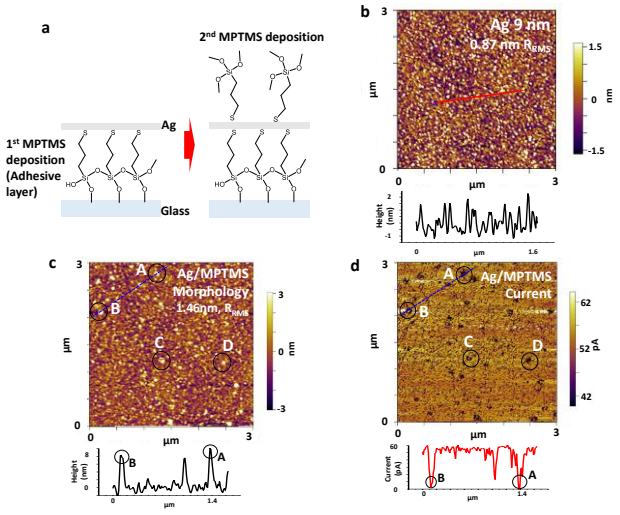

Figure 1: (a) Schematic of an MPTMS Ag seed layer (1st) and MPTMS capping layer (2nd) on either side of an optically thin Ag film; **(b)** AFM image of a 9 nm thick Ag film on MPTMS (1st layer) derivatized glass. **(c) & (d)** Conductive-AFM images of the morphology (c) and current (d) acquired simultaneously on a Ag electrode modified with an MPTMS layer (2nd layer). Image (d) was collected with an offset current of -53 pA. In (c) four mounds are highlighted by black circles A, B, C and D. In (d) the variation in conductance across mounds A and B is also shown. It is clear from (d) that these mounds are much less conductive than the surrounding area.

X-ray photoelectron spectroscopy (XPS) was used to determine the average thickness of the MPTMS layer on the Ag surface and to confirm the nature of the chemical bond between them. The high resolution XPS data in Figures 2(a) and (b) and survey scan in Figure S5b show no evidence of Si or S at the surface of the 9 nm-thick Ag film supported on MPTMS-derivatized

glass, and the asymmetry in the peak assigned to Ag 4s in Figure 2a is the same as that recorded for a pristine Ag film (Figure S5a). Based on the inelastic mean-free path of photoelectrons ejected from the Ag 3d orbital ~95 % of ejected electrons come from the top 3 - 4 nm of the Ag electrode.[17-19] The absence of peaks indicative of underlying glass and the MPTMS adhesion layer is compelling evidence that the 9 nm Ag film is compact and pin-hole free, such that the MPTMS adhesion layer and glass are completely buried by the Ag film. After the second MPTMS vapour deposition both Si and S are clearly present in the XPS spectrum taken from the surface of the 9 nm Ag film (Figure 2). In the S 2p binding energy region in Figure 2 there are two doublets consistent with two distinct chemical environments for the S.[20] Based on the intensity and binding energies of each pair, sulfur exists primarily as a thiolate covalently bound to Ag and the minor component is free thiol or disulphide. Given that 8 % of the surface comprises polymerised aggregation of MPTMS with a height equivalent to several MPTMS molecules it is plausible that the free thiol is associated primarily with these localised mounds. There is one dominant peak in the O 1s spectrum of MPTMS on Ag (Supporting Information Figure S5c) that is assigned to oxygen bound to Si and Me and / or O bound to Si and H.[21, 22] The minor peak is assigned to siloxane linkages which are expected to be present at the 8 % of the surface where there are MPTMS mounds. Collectively these data indicate that the MPTMS is primarily not cross-linked and from the attenuation of the Ag signal by the MPTMS layer the average thickness is 0.9 ± 0.1 nm (see Supporting Information for details of the calculation) which is fractionally higher than would be expected for a dense monolayer of MPTMS molecules: 0.7 - 0.8 nm.[15] Given that this is an average thickness, including the 8 % of the surface with MPTMS multilayers, this thickness is consistent with a monolayer over 92 % of the surface. Further indirect evidence that MPTMS is adsorbed at the surface is provided by the large change in work function from 4.59 ± 0.02 eV to 4.19 ± 0.06 eV, measured using photoelectron spectroscopy in Figure 2c. The large reduction in work function is consistent

with the perturbation of the surface dipole at the Ag surface due to the push-back effect.[23] The surface energy of the Ag film after MPTMS deposition is also reduced by one third from ~60 mJ/m^2 to ~40 mJ/m^2 (Figure 2d). Without the MPTMS capping layer the surface energy is strongly dependent on the time exposed to the ambient air, because the high surface energy of pristine metal results in physisorption of water and hydrocarbons from the atmosphere.

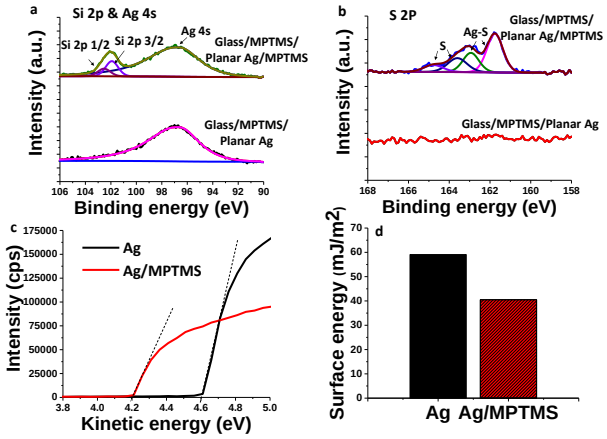

Figure 2. Surface analysis of Ag films with and without an MPTMS capping layer: High resolution XPS of the Si 2p and Ag 4s binding energy regions **(a)** and S 2p region **(b)**. The UPS secondary electron cut-off region **(c)** for Ag films with (red) and without (black) an MPTMS capping layer. **(d)** The average surface energy of bare Ag and Ag capped with MPTMS determined from static water contact angle measurement (Supporting Information, Figure S6).

Evaluating thin Ag film stability

Figure 3a shows the sheet resistance of 9 nm thick Ag film stored in ambient air over 620 hours (3.7 weeks) from which it is evident that the MPTMS capping layer at the Ag surface imparts

dramatically improved stability: The sheet resistance of MPTMS capped electrodes has increases by only 3%, from ~6.7 Ohms sq^{-1} to ~6.9 Ohms sq^{-1}, which is equivalent to rate of 0.008 Ohms sq^{-1} per day. Conversely without an MPTMS capping layer the sheet resistance increases an order of magnitude more quickly (0.1 Ohms sq^{-1} per day) reaching 9.6 Ohms sq^{-1} after 620 hours, a 40 % increase from its initial value. The latter can be attributed to morphological instability and oxidation both by molecular oxygen and airborne sulphurous compounds.[12, 13, 24] Small angle x-ray scattering (SAXS) analysis reveals that Ag films supported on MPTMS derivatized glass actually comprise a densely packed array of Ag particles with diameter of ~24 nm (Figure 3a inset). It is known that at room temperature diffusion of Ag atoms at the surface of small Ag crystallites enables the crystallites to deform like liquid drops to minimize their surface energy whilst retaining a highly crystalline core, and so electron transport between adjacent crystallites gradually deteriorates.[25] SI Figures S4a and 4c show that even after only 336 hours (2 weeks) the surface roughness of 9 nm Ag films has increased by 30 % percent. Over the same time period films with an MPTMS monolayer exhibit no significant change in the surface roughness: SI Figures S4b and 4d. The effectiveness of the MPTMS capping layer at imparting morphological stability can be understood at the macroscopic level in terms of the large reduction in surface energy, which reduces the thermodynamic driver for Ag crystallites to adopt a spherical shape. At the nanoscale those atoms bound to MPTMS molecules will be substantially less mobile than those without, hindering the surface diffusion need to bring around evolution of crystallite size.

For practical application in OPVs the transparent substrate electrode is coated with a semiconductor layer, most typically poly(3,4 ethylenedioxythiophene):poly(styrenesulfonate) (PEDOT:PSS) which must be briefly annealed in air at 100 - 140 ^{o}C to drive off the water used as the solvent. Consequently the thermal stability of Ag films towards low temperature annealing is of practical importance. It is evident from Figure 3b that the MPTMS layer

dramatically improves the stability of the electrode towards annealing, with no change in sheet resistance upon annealing up to 140 °C for 30 minutes.

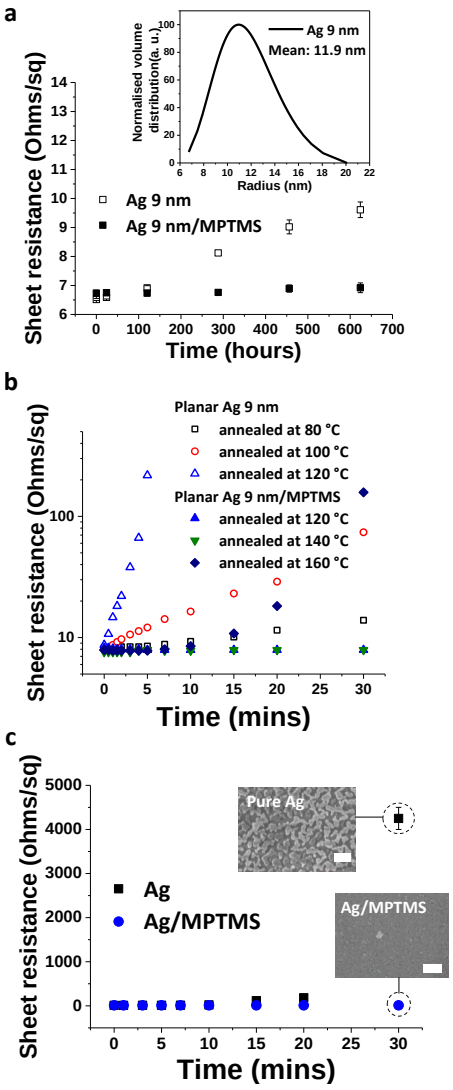

Figure 3. Stability testing of 9 nm Ag films with and without MPTMS capping layers: **(a)** Sheet resistance upon storage in ambient air.; **(a)** (inset) The size distribution of Ag crystallites making up the 9 nm Ag film on MPTMS-derivatized glass determined using small angle x-ray scattering.; **(b)** Sheet resistance of Ag and Ag / MPTMS films at different annealing temperatures.; **(c)** The sheet resistance of 9 nm Ag and Ag / MPTMS films heated at 80 °C in

sulfur gas.; **(c)** inset, SEM images show the morphologies of Ag and MPTMS-modified Ag films after exposure to sulfur gas for 30 minutes. The scale bars is 200 nm.

It is well-known that Ag is susceptible to oxidation by airborne sulphur compounds as well as oxygen, which is a serious problem for the long term stability of transparent electrodes based on optically thin silver films and nanowires.[13, 26] Upon exposure to sulphur gas (formed by heated sulphur at 80 ºC in air) the sheet resistance of bare Ag films increases to > 4000 Ohms sq^{-1} after 30 minutes: Figure 3c. SEM images of the Ag film after treatment with sulfur reveal that this correlates with a dramatic deterioration in the film morphology such that it has almost completely broken up, which is almost certainly accompanied by AgS formation.[26-28] Conversely MPTMS capped films exhibit only a small increase in sheet resistance of ~2 Ohms sq^{-1}, and no significant change in film morphology. It is remarkable that a single layer of MPTMS (over 92 % of the Ag surface) can block reaction with sulfur so effectively, given that even for a compact MPTMS monolayer only a fraction of the Ag atoms at the surface will have formed a thiolate linkage with MPTMS molecules.[29] This is compelling evidence that steric hindrance must also be an important factor in blocking reaction with gas phase sulphur. This finding is analogous to our previous report that the small molecule 3-mercaptopropylcarboxylic acid is particularly effective at retarding oxidation of copper nanoparticles in air.[30]

High performance OPV devices fabricated using stabilised Ag/MPTMS

In principle the MPTMS monolayer is thin enough not to impede the flow of charge to and from the Ag electrode. To test this hypothesis OPV devices with the architecture Glass / WO_3 (30 nm) / Ag (13 nm) (with and without MPTMS) / sol-gel ZnO / PBDB-T (PCE-

12):ITIC:$PC_{70}BM$ / MoO_3 / Ag, were fabricated and tested under 1 sun simulated solar illumination. Liu *et al.* have previously reported the use of the same ternary blend bulk heterojunction to fabricate OPVs with 10.6 % power conversion efficiency.[31] The sheet resistance of the 13 nm Ag electrode is ~4 Ohms sq^{-1}, a factor of three lower than the ITO glass used in this study. In this context the WO_3 layer serves as a metal nucleation layer as well as the anti-reflection layer to maximise the light coupling into the photoactive layer, and so an MPTMS metal nucleation layer was not needed. To our knowledge this is the first time that a WO_3 layer has been used in conjunction with a sol-gel ZnO layer to improve the transparency of an optically thin Ag electrode for OPVs. It is clear from the current-voltage characteristic in Figure 4 shows that the MPTMS layer does not contribute to an increase in device series resistance, since the gradient of the light curve where it crosses the voltage axis is not decreased. In fact, the device fill-factor (*FF*) is slightly improved upon inclusion of the MPTMS layer from 66.8 % ± 0.1 to 71.4 ± 0.3 % (Table 1). This small improvement is consistent with a reduction in the barrier to electron extraction across the Ag / ZnO interface, since the work function of the Ag electrode is reduced from ~4.6 eV to ~4.2 eV when derivatized with an MPTMS layer (Figure 2c), so that it is more closely matched to the conduction band edge in the ZnO.[32, 33] The J_{sc} for devices including an MPTMS layer is increased by 1.7 mA/cm^2, enabling a power conversion efficiency of 9.6 % ± 0.2 % (champion 10.0 %) to be achieved, which is comparable to that of devices using a conventional ITO glass electrode; 10.0 % ± 0.3 % (champion 10.6 %). This improvement in J_{sc} can also be attributed to a lower resistance to electron extraction across the Ag / ZnO interface due to reduced Schottky barrier height. Interestingly however, measurement of the transparency reveals that electrodes including an MPTMS layer at the Ag surface are actually substantially less transparent for wavelength > 500 nm due to increased reflectivity (Figure 5a). Whilst this reduces the amount of light let into the device, the increased reflectivity also operates to

improve trapping of light between the electrodes, via the micro-cavity effect,[31,34] which can easily outweigh the disadvantage of the loss in transparency in high performance OPVs due to the very thin photoactive layer. The differences in the shape of the EQE spectra (Figure 4 (inset)) are therefore a convolution of improved charge carrier extraction and micro-cavity effects.

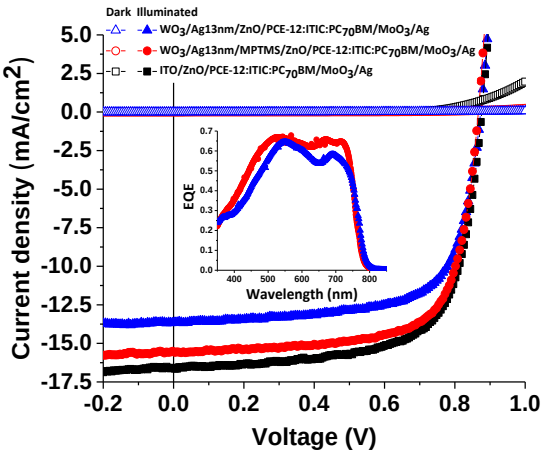

Figure 4. Representative *J-V* curves for OPV devices with the structure: glass / transparent conducting electrode / ZnO / PBDB-T (PCE-12):ITIC:$PC_{70}BM$ / MoO_3 / Ag (150 nm), where the transparent conducting electrode is: ITO (black); WO_3 (30 nm) / Ag (13 nm) (blue) and WO_3 (30 nm) / Ag (13 nm) / MPTMS (red). The inset shows the corresponding EQE for the devices with Ag window electrodes.

Table 1. Summary of photovoltaic device performance for devices with the structure: glass / transparent conducting electrode / ZnO / PBDB-T (PCE-12):ITIC:$PC_{70}BM$ / MoO_3 / Ag (150 nm), where the transparent conducting electrode is: ITO (black); WO_3 (30 nm) / Ag (13 nm)

(blue) and WO_3 (30 nm) / Ag (13 nm) / MPTMS (red). Errors are given as ± one standard deviation.

Window Electrodes	J_{SC} (mA/cm^2)	V_{OC} (mV)	FF (%)	Efficiency (%) (Max.)
WO_3 / Ag	13.7 ± 0.7	872.7 ± 16.6	66.8 ± 0.1	8.0 ± 1.1 (9.1)
WO_3 / Ag / MPTMS	15.4 ± 0.3	873.4 ± 7.9	71.4 ± 0.3	9.6 ± 0.2 (10.0)
ITO	16.3 ± 0.3	882 ± 10.0	69.3 ± 0.9	10.0 ± 0.3 (10.6)

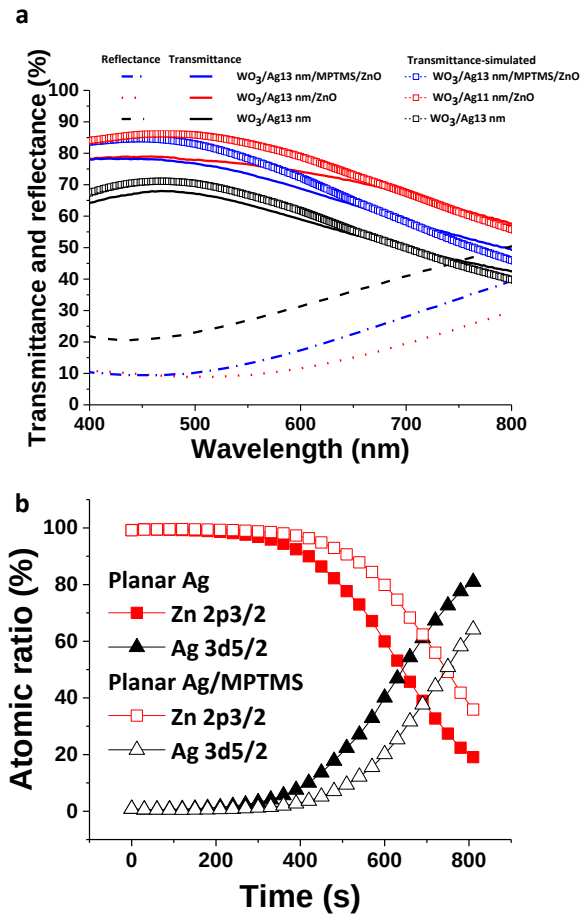

Figure 5. (a) Reflectance and transmittance spectra of: (blue) glass / WO_3 (30 nm) / Ag (13 nm) / MPTMS / ZnO (27 nm); (red) glass / WO_3 (30 nm) / Ag (13 nm) / ZnO (27 nm); (black) glass / WO_3 (30 nm) / Ag (13 nm). **(b)** Summary of XPS depth profile analysis of: (filled shapes) glass / WO_3 (30 nm) / Ag (13 nm) / ZnO (27 nm); (empty shapes) glass / WO_3 (30 nm) / Ag (13 nm) / MPTMS / ZnO (27 nm). The ZnO layer was etched by Ar^+ sputtering in 30 s

steps for a total etching time of 810 s. The Zn $2p_{3/2}$ and Ag $3d_{5/2}$ photoelectrons have been used to probe for Zn and Ag.

The reflectivity of the WO_3 / Ag / ZnO electrode is strongly dependant on the refractive index of the oxide layers on either side of the metal film, which can be substantially altered when these oxides are doped with metals.[6] In this case the only difference between the two electrodes is the presence of the MPTMS layer at the Ag / ZnO interface. It is known that Ag diffuses into ZnO and so the difference in reflectivity could stem from a difference in the extent to which Ag diffuses into the adjacent ZnO layer, with and without the MPTMS layer.[35] To investigate this hypothesis we have used XPS depth profiling with argon ion sputtering. Figure 5 shows the results of depth profiling of Ag (13 nm) capped with a ZnO (30 nm) layer with and without MPTMS at the Ag / ZnO interface. It is clear from these data that Ag is detected substantially earlier when there is no MPTMS layer, which is compelling evidence that the MPTMS layer serves to suppress Ag diffuse into the ZnO layer. This result is consistent with the observation that the sheet resistance of Ag / ZnO films also increases after annealing, whilst that of Ag / MPTMS / ZnO does not (SI, Table S2.), because the sheet resistance of the bilayer electrode will be primarily determined by that of the Ag film, and so loss of Ag into the ZnO layer will inevitably erode the sheet resistance of the bilayer.

One key advantage of metal film electrodes over conventional conducting oxide electrodes such as ITO, is their compatibility with flexible plastic substrates.[5] To test this for the electrode described herein, we have fabricated electrodes with the structure WO_3 / Ag (13 nm) / MPTMS / ZnO electrodes on 125 μm PET, and compared the evolution in sheet resistance to that of commercial ITO coated plastic (Teonix Q51 PEN 15 Ohms sq^{-1}) when repeatedly bent through a radius of curve of 4 mm: Supporting Information Figure S7. Within error the

sheet resistance of the oxide-metal-oxide electrode is unchanged after 100 bending cycles, whether the stress is tensile or compressive. In contrast the sheet resistance of the ITO electrode dramatically increases upon bending, most rapidly when the stress is tensile.

The long term degradation of OPVs depends on a number of parallel degradation mechanisms which makes it difficult to isolate the contribution of improved stability of the Ag electrode when buried between multiple layers. However, optically thin Ag electrodes are also attractive as the transparent electrode in OPVs with a top-illuminated architecture, and so semi-transparent OPVs with the structure ITO / ZnO (sol-gel) / PBDB-T:ITIC:$PC_{70}BM$ / MoO_3 / Ag (9 nm) were tested under constant illumination in N_2, with and without an MPTMS layer on the outermost surface of the Ag electrode. This device architecture has an average transparency of 32 % across the visible spectrum (Figure 6a). After 6 hours constant 1 sun simulated solar illumination the performance of devices without an MPTMS capping layer start to deteriorate rapidly (Figure 6b). After a further 2 hours the power conversion efficiency is < 1 %, which correlates with major morphological deterioration of the top Ag electrode: Figure 6b (inset). Over the same test period devices with an MPTMS capping layer do not exhibit a sharp deterioration in performance, and the extent of morphological evolution of the top electrode is substantially reduced (Figure 6b inset), consistent with the stabilising effect of the ultra-thin MPTMS capping layer.

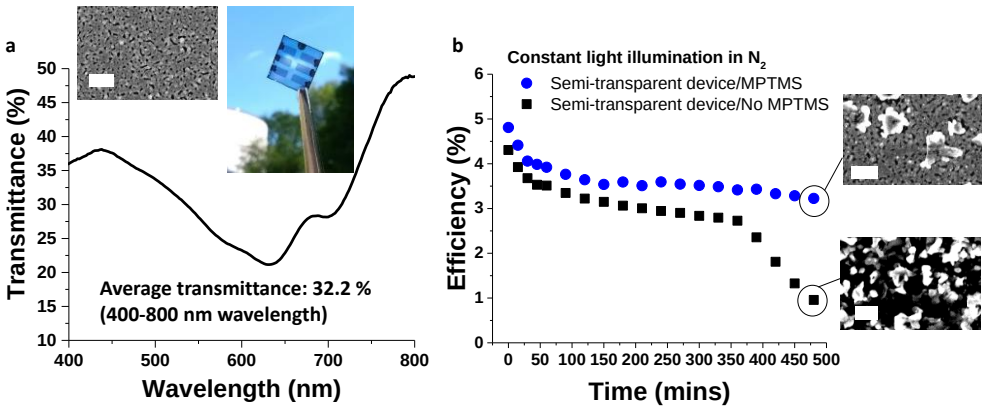

Figure 6. Semi-transparent organic photovoltaic devices with the structure: glass / WO_3 (30 nm) / Ag (13 nm) (with and without MPTMS) / ZnO / PBDB-T (PCE-12):ITIC:$PC_{70}BM$ / MoO_3 / Ag (9 nm). **(a)** Far-field transmittance spectra showing average transparency across the visible spectrum of 32 %. Also shown is an SEM image of the top of the 9 nm-thick Ag electrode and a photograph of the device. (b) Constant illumination stability test in N_2, under 1 sun simulated solar with illumination from the glass slide. The inset SEM images show the morphological deformation of the 9 nm Ag electrode. The scale bar is 200 nm for all the SEM images.

CONCLUSIONS

In summary, a ~1 nm layer of 3-mercaptopropyltrimethoxysilane at the surface of transparent Ag films is found to be remarkably effective at suppressing Ag film degradation due to spontaneous morphological evolution and oxidation by airborne sulphur. Inclusion of this layer at the Ag / ZnO interface in a triple layer electrode WO_3 / Ag / ZnO results in ~20 % improvement in power conversion efficiency, such that the efficiency is comparable to that achieved using an ITO glass electrode: 9.6 ± 0.2 *vs* 10.0 ± 0.3, with the advantage that the Ag electrode has a sheet resistance of ~4 Ohms sq^{-1} - one third that of the ITO glass used in this

study. In this context the MPTMS layer is shown to result from the MPTMS blocking Ag diffusion into the adjacent ZnO layer, and from a favourable ~400 meV reduction in the Ag electrode work function. In addition to its utility inside the OPV device, we have also shown that an ultra-thin MPTMS layer is useful for improving the stability of the top-silver electrode in semi-transparent OPVs, since it can be deposited onto the device from the vapour phase forming a conformal coating. Notably, in this work the MPTMS nanolayer was deposited from the vapour phase at a temperature well below its boiling point. However, for practical applications it is reasonable to expect that the rate of deposition could be dramatically increased by raising the temperature.

Experimental

Materials: MPTMS (95 %) and zinc acetate dehydrate (≥ 90 %) were purchased from Sigma-Aldrich. 2-Methoxyethanol (99 %) and ethanolamine (99+ %) were purchased from Alfa Aesar. PCE12 (Poly[(2,6-(4,8-bis(5-(2-ethylhexyl)thiophen-2-yl)-benzo[1,2-b:4,5-b']dithiophene))-alt-(5,5-(1',3'-di-2-thienyl-5',7'-bis(2-ethylhexyl)benzo[1',2'-c:4',5'-c']dithiophene-4,8-dione)]), ITIC (3,9-bis(2-methylene-(3-(1,1-dicyanomethylene)-indanone))-5,5,11,11-tetrakis(4-hexylphenyl)-dithieno[2,3-d:2',3'-d']-s-indaceno[1,2-b:5,6-b']dithiophene) and $PC_{70}BM$ ([6,6]-Phenyl-C_{71}-butyric acid methyl ester) were purchased from Ossila Ltd. All the materials were used as received.

MPTMS deposition: Glass substrates were ultrasonically agitated in an aqueous surfactant solution (Hellmanex iii), boiling deionised water and isopropyl alcohol for 10 mins in each case. The substrate was then UV-ozone cleaned for 15 mins and transferred into a crystallisation dish with a closed lid for the 1st MPTMS deposition (i.e. the metal seed layer).

The MPTMS nucleation layer was deposited at ambient pressure from the vapour phase with heating at 100 ºC. Unless otherwise stated, this treatment was performed for 16 hours. Vapour phase chemical derivatization of the glass surface was followed by ultra-sonic agitation in ethanol for 30 mins to remove physisorbed MPTMS and any multi-layers prior to vacuum evaporation of Ag films.

For the 2nd MPTMS deposition, Ag films were placed in a PTFE holder and transferred into a sealed crystallizing dish together with a small vial containing a few drops of MPTMS. The bottom of the crystallizing dish was heated to 100 ºC, but the sample (being significantly thermally isolated by the PTFE holder) was not heated beyond 50 ºC as measured using a thermal imaging camera. This process can be performed in ambient air or a nitrogen atmosphere. In the case of glass / WO_3 / Ag films, the WO_3 layer served as the metal seed layer and so a MPTMS seed layer (1st layer) was not required. Electrodes were taken out of the vacuum chamber for the 2nd MPTMS deposition, which was performed in a N_2 filled glove box using the previously reported desiccator deposition method.[15] It was found that the ZnO wetted the MPTMS derivatized surface more readily after rinsing the electrode in warm (~65 ºC) deionised water for 20 mins, a process that results in hydrolysis of the MPTMS molecules.[21]

OPV device fabrication: The zinc acetate solution was spin coated on ITO, WO_3 / Ag, and WO_3 / Ag / MPTMS electrodes and annealed at 150 ºC for 30 mins in air, to achieve a ZnO film thickness of ~27 nm. The ZnO solution was prepared as reported in reference 36. A PCE12:ITIC:$PC_{70}BM$ ternary blend (1:0.5:0.5, 20 mg/ml) was dissolved in chlorobenzene with 0.5 v% of 1,8-diiodooctane (DIO) and gently heated at 50 °C overnight. Then the blend was spin-coated at 3000 rpm to obtain a 90 nm-thick photoactive layer. MoO_3 (10 nm, 0.2 Å/s) and Ag (150 nm, 1 Å/s) films were deposited by thermal evaporation under 2×10^{-6} mbar vacuum pressure to complete the device.

Characterisation and measurement: The morphology of films was probed using an MFP-3D AFM (Asylum Research) and the optical characteristics were measured by Lambda 1050 (PerkinElmer) and Cary 60 (Agilent Technologies) UV-Vis Spectrophotometer. The sheet resistance of the electrodes was calculated from the current measured by Keithley 2400 Sourcemeter using Van der Pauw method. OPV characteristics were measured under 1 Sun illumination using 0.0288 cm^2 area pixel masks. The contact angle was measured using DSA100 drop shape analyser (Krüss) with 1 or 2 µl of DI water. The surface energy was calculated using the method in references 37 and 38.

The XPS and UPS analysis were performed using a Kratos AXIS Ultra DLD. The depth profile was performed by etching samples by Ar^+ sputtering in 30 second steps for a total etching time of 810 seconds and scanning the Zn $2p_{3/2}$ and Ag $3d_{5/2}$ binding energy regions. The data were analysed in the CasaXPS package using Shirley backgrounds and mixed Gaussian-Lorentzian (Voigt) lineshapes, with asymmetry parameters employed where appropriate.

Grazing incidence small-angle X-ray scattering (GISAXS) measurements were made using a Xenocs Xeuss 2.0 equipped with a micro-focus Cu Kα source collimated with Scatterless slits. The scattering was measured using a Pilatus 300k detector with a pixel size of 0.172 mm × 0.172 mm. The distance between the detector and the sample was calibrated using silver behenate ($AgC_{22}H_{43}O_2$), giving a value of 2.480(5) m. The magnitude of the scattering vector (q) is given by $q=4\pi \sin(\theta)/\lambda$, where 2θ is the angle between the incident and scattered X-rays and λ is the wavelength of the incident X-rays. This gave a q range for the detector of 0.003 $Å^{-1}$ and 0.13 $Å^{-1}$ in the horizontal plane. This q range allows crystallite sizes between 1 and 200 nm to be determined. Samples were aligned such that the surface was parallel to the beam and in the center of the beam. To maximize the scattering signal from the Ag layer the

sample was positioned at an incidence angle (αi) of 0.45 ° which is just above the critical angle of 0.4 ° for Ag and Cu Kα radiation. The 2d detector image was integrated as a function of q producing a 1d intensity versus q data set. Selecting only in-plane scattering allows the horizontal radius of the crystallites to be determined. SAXS fitting was performed in the Irena analysis package.[39] The scattering was fitted using spheres with a lognormal distribution of the radius combined with a hard-sphere structure factor to model the interaction between crystallites.

AUTHOR INFORMATION

Corresponding Author

* E-mail: (Ross.Hatton@warwick.ac.uk)

ASSOCIATED CONTENT

Supporting Information

The Supporting Information is available free of charge on the ACS Publications website at DOI:xxxx

All data supporting this study are provided as supplementary information accompanying this paper: Details of optimization of the 1st MPTMS deposition; Transmittance spectra; Atomic force microscope images of surface topography; Calculation of the MPTMS monolayer thickness; X-ray photoelectron microscopy analysis; Contact Angle measurements; Sheet resistance measurements; Bending tests.

ACKNOWLEDGMENT

The authors would like to thank the United Kingdom Engineering and Physical Sciences Research Council (EPSRC) for funding (Grant number: EP/N009096/1).

REFERENCES

1. Cook, R. M.; Pegg, L.-J.; Kinnear, S. L.; Hutter, O. S.; Morris, R. J. H.; Hatton, R. A., An Electrode Design Rule for Organic Photovoltaics Elucidated Using Molecular Nanolayers. *Adv. Energy Mater.* **2011,** *1* (3), 440-447.
2. Beaumont, N.; Hancox, I.; Sullivan, P.; Hatton, R. A.; Jones, T. S., Increased efficiency in small molecule organic photovoltaic cells through electrode modification with self-assembled monolayers. *Energy Environ. Sci.* **2011,** *4* (5), 1708-1711.
3. Ha, Y. E.; Jo, M. Y.; Park, J.; Kang, Y.-C.; Yoo, S. I.; Kim, J. H., Inverted Type Polymer Solar Cells with Self-Assembled Monolayer Treated ZnO. *J. Phys. Chem. C* **2013,** *117* (6), 2646-2652.
4. Liu, L.; Mei, A.; Liu, T.; Jiang, P.; Sheng, Y.; Zhang, L.; Han, H., Fully Printable Mesoscopic Perovskite Solar Cells with Organic Silane Self-Assembled Monolayer. *J. Am. Chem. Soc.* **2015,** *137* (5), 1790-1793.
5. Stec, H. M.; Hatton, R. A., Widely Applicable Coinage Metal Window Electrodes on Flexible Polyester Substrates Applied to Organic Photovoltaics. *ACS Appl. Mater. Interfaces* **2012,** *4* (11), 6013-6020.
6. Hutter, O. S., Hatton, R. A., Hybrid Copper:Tungsten Suboxide Window Electrode for Organic Photovoltaics. *Adv. Mater.* ***2017,*** 27, 326-331.
7. Babar, S.; Weaver, J. H., Optical constants of Cu, Ag, and Au revisited. *Appl. Opt.* **2015,** *54* (3), 477-481.
8. Johnson, P. B.; Christy, R. W., Optical Constants of the Noble Metals. *Phys. Rev. B* **1972,** *6* (12), 4370-4379.
9. Ordal, M. A.; Bell, R. J.; Alexander, R. W.; Long, L. L.; Querry, M. R., Optical properties of fourteen metals in the infrared and far infrared: Al, Co, Cu, Au, Fe, Pb, Mo, Ni, Pd, Pt, Ag, Ti, V, and W. *Appl. Opt.* **1985,** *24* (24), 4493-4499.
10. Krebs, F. C.; Espinosa, N.; Hosel, M.; Sondergaard, R. R.; Jorgensen, M., 25th Anniversary Article: Rise to Power - OPV-Based Solar Parks. *Adv. Mater.* **2014,** *26* (1), 29-39.
11. Cho, J. H.; Lim, J. A.; Han, J. T.; Jang, H. W.; Lee, J. L.; Cho, K., Control of the electrical and adhesion properties of metal/organic interfaces with self-assembled monolayers. *Appl. Phys. Lett.* **2005,** *86* (17), 171906
12. Zhang, C.; Kinsey, N.; Chen, L.; Ji, C.; Xu, M.; Ferrera, M.; Pan, X.; Shalaev, V. M.; Boltasseva, A.; Guo, L. J., High-Performance Doped Silver Films: Overcoming Fundamental Material Limits for Nanophotonic Applications. *Adv. Mater.* **2017,** *29* (19), 1605177.
13. Bellchambers, P.; Lee, J.; Varagnolo, S.; Amari, H.; Walker, M.; Hatton, R. A., Elucidating the Exceptional Passivation Effect of 0.8 nm Evaporated Aluminium on Transparent Copper Films. *Front. Mater.* **2018,** *5*, 71.
14. Kang, H.; Jung, S.; Jeong, S.; Kim, G.; Lee, K., Polymer-metal hybrid transparent electrodes for flexible electronics. *Nat. Commun.* **2015,** *6*, 6503.
15. Stec, H. M.; Williams, R. J.; Jones, T. S.; Hatton, R. A., Ultrathin Transparent Au Electrodes for Organic Photovoltaics Fabricated Using a Mixed Mono-Molecular Nucleation Layer. *Adv. Funct. Mater.* **2011,** *21* (9), 1709-1716.

16. Hatton, R. A.; Willis, M. R.; Chesters, M. A.; Briggs, D., A robust ultrathin, transparent gold electrode tailored for hole injection into organic light-emitting diodes. *J. Mater. Chem.* **2003,** *13* (4), 722-726.
17. Kawai, J.; Adachi, H.; Kitajima, Y.; Maeda, K.; Hayakawa, S.; Gohshi, Y., Inelastic mean free path of photoelectrons in Ag determined by total reflection X-ray photoelectron spectroscopy. *Anal. Sci.* **1997,** *13* (5), 797-801.
18. S. Tanuma, C. J. P., and D. R. Penn, Calculations of electron inelastic mean free paths. V. Data for 14 organic compounds over the 50–2000 eV range. *Surf. Interface Anal.* **1994,** *21* (3), 165-176.
19. Jablonski, A.; Tougaard, S., Comparison of the attenuation lengths and the inelastic mean-free path for photoelectrons in silver. *J. Vac. Sci. Technol* **1990,** *8* (1), 106-116.
20. Tyler, M. S.; Walker, M.; Hatton, R. A., High-Performance Silver Window Electrodes for Top-Illuminated Organic Photovoltaics Using an Organo-molybdenum Oxide Bronze Interlayer. *ACS Appl. Mater. Interfaces* **2016,** *8* (19), 12316-12323.
21. Thompson, W. R.; Cai, M.; Ho, M. K.; Pemberton, J. E., Hydrolysis and condensation of self-assembled monolayers of (3-mercaptopropyl)trimethoxysilane on Ag and Au surfaces. *Langmuir* **1997,** *13* (8), 2291-2302.
22. Sinapi, F.; Delhalle, J.; Mekhalif, Z., XPS and electrochemical evaluation of two-dimensional organic films obtained by chemical modification of self-assembled monolayers of (3-mercaptopropyl)trimethoxysilane on copper surfaces. *Mater. Sci. Eng., C* **2002,** *22* (2), 345-353.
23. Ishii, H.; Sugiyama, K.; Ito, E.; Seki, K., Energy level alignment and interfacial electronic structures at organic/metal and organic/organic interfaces (vol 11, pg 605, 1999). *Adv. Mater.* **1999,** *11* (12), 972-972.
24. Sanders, C. E.; Verreault, D.; Frankel, G. S.; Allen, H. C., The Role of Sulfur in the Atmospheric Corrosion of Silver. *J. Electrochem. Soc.* **2015,** *162* (12), C630-C637.
25. Sun, J.; He, L.; Lo, Y.-C.; Xu, T.; Bi, H.; Sun, L.; Zhang, Z.; Mao, S. X.; Li, J., Liquid-like pseudoelasticity of sub-10-nm crystalline silver particles. *Nat. Mater.* **2014,** *13* (11), 1007-1012.
26. Eom, H.; Lee, J.; Pichitpajongkit, A.; Amjadi, M.; Jeong, J.-H.; Lee, E.; Lee, J.-Y.; Park, I., Ag@Ni Core-Shell Nanowire Network for Robust Transparent Electrodes Against Oxidation and Sulfurization. *Small* **2014,** *10* (20), 4171-4181.
27. Ayhan, M. E.; Kalita, G.; Sharma, S.; Tanemura, M., Chemical vapor deposition of graphene on silver foil as a tarnish-resistant coating. *Phys. Status Solidi Rapid Res. Lett.* **2013,** *7* (12), 1076-1079.
28. Sinclair, J. D., Tarnishing of silver by organic sulfur vapors: rates and film characteristics. *J. Electrochem. Soc.* **1982,** *129* (1), 33-40.
29. Love, J. C.; Estroff, L. A.; Kriebel, J. K.; Nuzzo, R. G.; Whitesides, G. M., Self-assembled monolayers of thiolates on metals as a form of nanotechnology. *Chem. Rev.* **2005,** *105* (4), 1103-1169.
30. Dabera, G.; Walker, M.; Sanchez, A. M.; Pereira, H. J.; Beanland, R.; Hatton, R. A., Retarding oxidation of copper nanoparticles without electrical isolation and the size dependence of work function. *Nat. Commun.* **2017,** *8*, 1894.
31. Liu, Q.; Toudert, J.; Ciammaruchi, L.; Martinez-Denegri, G.; Martorell, J., High open-circuit voltage and short-circuit current flexible polymer solar cells using ternary blends and ultrathin Ag-based transparent electrodes. *J. Mater. Chem. A* **2017,** *5* (48), 25476-25484.
32. Liang, Z.; Zhang, Q.; Wiranwetchayan, O.; Xi, J.; Yang, Z.; Park, K.; Li, C.; Cao, G., Effects of the Morphology of a ZnO Buffer Layer on the Photovoltaic Performance of Inverted Polymer Solar Cells. *Adv. Funct. Mater.* **2012,** *22* (10), 2194-2201.

33. Kyaw, A. K. K.; Sun, X. W.; Jiang, C. Y.; Lo, G. Q.; Zhao, D. W.; Kwong, D. L., An inverted organic solar cell employing a sol-gel derived ZnO electron selective layer and thermal evaporated MoO3 hole selective layer. *Appl. Phys. Lett.* **2008,** *93* (22), 221107
34. Armin, A.; Velusamy, M.; Wolfer, P.; Zhang, Y.; Burn, P. L.; Meredith, P.; Pivrikas, A., Quantum Efficiency of Organic Solar Cells: Electro-Optical Cavity Considerations. *ACS Photonics* **2014,** *1* (3), 173-181.
35. Wang, T.; Bristowe, P. D., Controlling Ag diffusion in ZnO by donor doping: A first principles study. *Acta Mater.* **2017,** *137*, 115-122.
36. Sun, Y.; Seo, J. H.; Takacs, C. J.; Seifter, J.; Heeger, A. J., Inverted polymer solar cells integrated with a low-temperature-annealed sol-gel-derived ZnO Film as an electron transport layer. *Adv. Mater.* **2011,** 23 (14), 1679-1683.
37. Paniagua, S. A.; Hotchkiss, P. J.; Jones, S. C.; Marder, S. R.; Mudalige, A.; Marrikar, F. S.; Pemberton, J. E.; Armstrong, N. R., Phosphonic acid modification of indium-tin oxide electrodes: Combined XPS/UPS/contact angle studies. *J. Phys. Chem. C* **2008,** 112 (21), 7809-7817.
38. Ma, K. X.; Ho, C. H.; Zhu, F. R.; Chung, T. S., Investigation of surface energy for organic light emitting polymers and indium tin oxide. *Thin Solid Films* **2000,** 371 (1-2), 140-147.
39. Ilavsky, Jan; Jemian, Peter R., Irena: tool suite for modeling and analysis of small-angle scattering. *J. Appl. Cryst.* **2009,** 42 (2), 347-353.